Journal of Alloys and Compounds 521 (2012) 50–54

Contents lists available at SciVerse ScienceDirect

Journal of Alloys and Compounds

journal homepage: www.elsevier.com/locate/jallcom

Determination of the Mn^{3+}/Mn^{4+} ratio in $La_{1-x}Sr_xMnO_{3\pm d}$ powders

Guilherme Oliveira Siqueira, Rose Marie Belardi, Pedro Hespanha Almeida, Charles Luís da Silva, Márcia Caldeira Brant, Tulio Matencio, Rosana Zacarias Domingues *

Departamento de Química, ICEx – Universidade Federal de Minas Gerais, Av. Antônio Carlos, 6627, CEP 31270-90, Belo Horizonte, Brazil

ARTICLE INFO

Article history:
Received 14 August 2008
Received in revised form
30 December 2011
Accepted 4 January 2012
Available online 21 January 2012

Keywords:
Electrode materials
Chemical synthesis
Powder metallurgy
X-ray diffraction
Electronic transport

ABSTRACT

The present work combines the results of two simple methods of determination of the Mn^{3+}/Mn^{4+} ratio for $La_{1-x}Sr_xMnO_{3\pm d}$ powders, prepared by citrate route, in which the Sr content, *x*, varies from 0.16 to 0.40. The ratio Mn^{3+}/Mn^{4+} was successfully estimated combining the results of Temperature Programmed Reduction (TPR) analysis and redox titration. Moreover, the possible perovskite chemical formulas were established and a direct relationship between the Sr content and the Mn^{4+} amount was found. Morphological analyses such as grain size and surface area are also presented to better characterize the powders. Gas adsorption by Brunauer–Emmett–Teller method (BET) and scanning electron microscopy (SEM) were used to evaluate the agglomeration degree of powders and showed the inhibitory influence of Sr content on the growth of crystallites.

1. Introduction

Strontium-doped lanthanum manganites (LSM) are perovskite-type oxides (ABO_3), with lanthanum and strontium in the A-site and Mn as a transition metal in the B-site. They have been widely studied mainly due to their interesting catalytic oxygen cathode reduction and mixed electronic–ionic conduction properties [1–4]. Most of these applications are related to the LSM ability to perform the adsorption and reduction of molecular oxygen, and the subsequent transport of the oxide ions formed [5–15]. The partial substitution of the lanthanum in $LaMnO_3$ by aliovalent cations, like Sr^{2+}, promotes morphological, chemical and crystallographic changes. The Mn—O bond length and Mn—O—Mn bond angle, the oxygen distribution, the number of cation vacancies and Mn^{3+}/Mn^{4+} concentrations are strongly affected by the Sr content [16–19]. For solid oxide fuel cell, SOFC, applications, $La_{1-x}Sr_xMnO_3$ is the most common material used as the due to its high electrical conductivity and good chemical and thermal compatibilities with the zirconia electrolytes. The best compositions have *x* content varying from 0.1 to 0.5 and according to many authors the electrical conductivity increases with an increase in the amount of Sr content [20,21]. For these specific applications, bulk and surfaces properties of LSM are both important since they control the process of adsorption, reduction and transport of oxygen species. Although the Sr solid solution, $La_{1-x}Sr_xMnO_3$, is known to occur for a large *x* extension, the Sr enrichment at the LSM surface has been evidenced by X-ray photoelectron spectroscopy according to the conditions of annealing (temperature, oxygen pressure) and polarization treatments [22]. The species present on LSM surface can also modify the catalytic properties and electrical conductivity of these materials. A recent study identified at least two species, attributed to O^{2-} and O_2^{2-} at 873 K on LSM surface.

The electric transport and magnetic properties of these manganites are closely related to the Mn oxidation state, which is determined by the oxygen content of the sample. Many authors suggest that the Mn^{3+}/Mn^{4+} ratio is a unique parameter for understanding the colossal magnetoresistance effect as well as the transition from the ferromagnetic metal to the paramagnetic. The accurate characterization of the nonstoichiometric oxide materials, mainly for the hole-doped manganese perovskites $Ln_{1-x}A_xMnO_3$ (Ln = La–Tb, and A = Ca, Sr, Ba), has been described in literature [23–32] but the methods used are often complex.

The present work compares the results of two simple methods of determination of the Mn^{3+}/Mn^{4+} ratio for LSM powders, prepared by citrate route, in which the Sr content varied from 0.16 to 0.40. The ratio Mn^{3+}/Mn^{4+} was estimated by temperature programmed reduction (TPR) analysis and by redox titration. As a result, the possible perovskite chemical formulas are given. Some morphological analyses such as grain size and surface area are also presented to better characterize the powders.

* Corresponding author. Tel.: +55 31 409 57 70; fax: +55 31 409 57 00.
E-mail address: rosanazd@ufmg.br (R.Z. Domingues).

0925-8388/$ – see front matter © 2012 Elsevier B.V. All rights reserved.
doi:10.1016/j.jallcom.2012.01.023

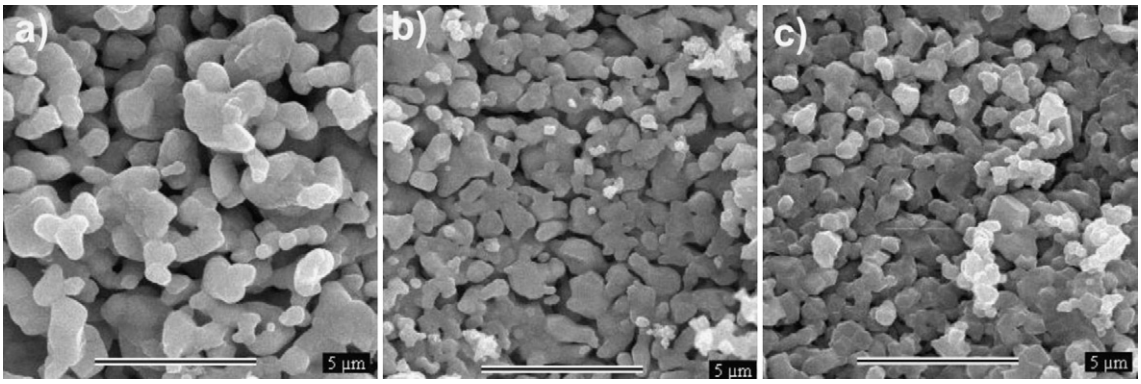

Fig. 1. SEM of samples: (a) LSM1; (b) LSM2; (c) LSM3.

2. Materials and methods

$La_{1-x}Sr_xMnO_3$ powders with three different stoichiometry compositions were obtained from a mixture of monohydrated citric acid (Vetec, 99.5%), strontium nitrate (Vetec, 99.0%), manganese acetate tetrahydrate (Vetec, 99.0%), and lanthanum nitrate hexahydrate (Vetec, 99.0%) by the amorphous citrate route. La, Sr, and Mn salts were dissolved in distillated water. Citric acid was added to this solution in a ratio of 1:2 to the metal content. This solution was magnetically stirred at 343 K until gelation. The obtained gel was ground to a powder, hereafter called LSM. Next, it was thermally treated at 423 K for 1 h. Cylindrical pellets were prepared by uniaxial pressing at approximately 390 MPa and subsequent sintering at 1473 K in air for 4 h. Their final dimensions were about 11 and 4 mm of diameter and thickness, respectively. LSM1, LSM2 and LSM3 labels correspond to $La_{1-x}Sr_xMnO_3$ powders with x equal to 0.16, 0.20, and 0.40, respectively.

The LSM powders were analyzed using a XRD (Rigaku model Geigerflex-3034 and a Siemens model D5000 diffractometers) with a Cu Ka radiation source. XRD data were treated by the Rietveld refinement method. Microstructural analyses were performed on the surface of LSM pellets.

An electron microprobe apparatus (JEOL model JXA-8900) was used in scanning electron microscopy (SEM) analysis. Particle grain sizes were estimated from SEM using image analysis software [33]. The specific surface area measurements were made by B.E.T. (Autosorb-Quantachrome model NOVA 1200).

Mn, Sr and La elements were quantified by ICP-MS and/or inductively coupled plasma atom emission spectrometry (ICP-AES) using a spectrometer, model Spectroflame (Spectro Analytical Instruments, Kleve, Germany).

The reduction behavior of samples with different Sr-concentration has been evaluated by temperature-programmed reduction (TPR). The experiment was carried out on a Quantachrome Chembet 3000 under 80 mL min^{-1} H_2 (5%) and N_2 mixture gas flow. The measurement was carried out in the temperature range 373–1173 K, at a heating rate of 10 K min^{-1} using 53 mg of powder samples. Quantitative analyses were performed by using CuO as standard.

The percentage of Mn^{4+} was also estimated by a redox back titration in which the powder sample was dissolved in a sulfuric acid aqueous solution containing an excess of sodium oxalate that was titrated with a permanganate standard solution. Details of the procedure are given in reference [34].

3. Results and discussions

Scanning electron micrographs of the pellets sintered at 1473 K reveals homogeneous and uniform aspect for all studied samples, as shown in Fig. 1. From these images the particle sizes were estimated using the quantikov image analyzer [33] and the average values are presented in Table 1.

LSM1 exhibits a grain size about 10 times higher than those obtained for LSM1 and LSM2 for which grain sizes are constant and measured about 0.8 μm. Higher Sr concentration seems to inhibit particle growth.

The superficial area of LSM powders seems not to be influenced by the strontium content. The values are about 3 m^2 g^{-1} and this is characteristic of not porous materials. These results are also given in Table 1.

Fig. 2 shows XRD diffractograms, obtained for LSM1 and LSM2 powders, sintered at 1473 K. The synthetic route used promoted the total crystallization of perovskite and no other phases were detected by the method used. XRD diffractograms of LSM3 powders sintered at the same temperature are also shown in Fig. 2. Despite the relatively high sinterization temperature (1473 K), peaks attributed to $La(OH)_3$ were observed.

Table 1
Some LSM parameters obtained from BET and DXR analysis.

	LSM1	LSM2	LSM3
Grain size (μm)	6(3)	0.9(3)	0.8(3)
Specific superficial area (m^2 g^{-1})	3(1)	3(1)	4(1)
a (Å)	5.5278(7)	5.5214(1)	5.5114(2)
b (Å)	5.5278	5.5214	5.4565(2)
c (Å)	13.3660(2)	13.3653(3)	7.7305(3)
Volume (Å^3)	353.69(1)	352.86 (1)	232.48(1)
Density (g cm^{-3})	6.5838	6.5411	6.1609
Perovskite (%$_{m/m}$)	100	100	94.19(2)
$La(OH)_3$ (%$_{m/m}$)	0	0	5.8(1)

In fact, several authors [37,41–43] identified the presence of a small amount of La_2O_3, $La(OH)_3$ or other secondary phases in similar studies. They suggested that, since the ion La^{3+} ionic radius is 1.46 Å while that of the ion Sr^{2+} is of 1.54 Å, the substitution of La^{3+} for Sr^{2+} in the structure type perovskite of $LaMnO_3$ is limited [37] and stronger Sr doping on LSM systems favors the formation of secondary phases.

Bell et al. [42], also suggested that the lower temperatures or lower calcinations duration are responsible for La_2O_3 formation. The presence of La_2O_3 in sample LSM3 could be associated to

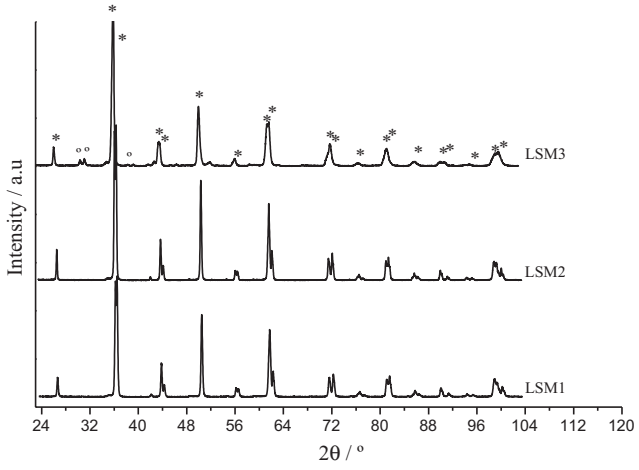

Fig. 2. XRD patterns of samples in which the symbols (*) denote perovskite peaks, and (○) denote $La(OH)_3$ peaks.

Table 2
ICP-MS results. Weight percent values of the elements in the sample and molar La:Sr:Mn ratio of the perovskite structure.

Sample	La ($\%_{w/w}$)	Sr ($\%_{w/w}$)	Mn ($\%_{w/w}$)	Molar ratios La:Sr:Mn
LSM1	50.8(5)	5.7(3)	22.2(5)	90:16:100
LSM2	48.4(5)	7.4(3)	22.9(5)	83:20:100
LSM3	40.6(5)	15.5(3)	24.9(5)	58:39:100

insufficient calcination time. Marques et al. [43] noted that La_2O_3 exposed to laboratory atmosphere absorbs water forming $La(OH)_3$ which may explain the presence of $La(OH)_3$ in sample LSM3 even after thermal process at 1473 K. In a more recent paper, Fleming et al. [44] described the reactivity of various lanthana powders in air and concluded that these materials rapidly hydroxylate to form a stable hydroxide, $La(OH)_3$, at room temperature.

LSM1 and LSM2 presented a trigonal structure with the symmetry group *R-3ch* and LSM3 presented a orthorhombic structure and a *Pbnm* symmetry group [35,36]. The lattice parameter errors for Rietveld analysis (results not shown) agree with those found in literature [37]. The lattice parameters of manganites doped with different strontium concentrations are given in Table 1. The unit cell volume decreases with increasing strontium concentration. As the parameter *a* is related to the distance of the Mn—O bonds and Mn^{4+} ions (0.530 Å) are smaller than Mn^{3+} ions (0.645 Å), the charge density of Mn^{4+} favors the contraction of Mn—O bonds [15,37,38]. Another factor that could contribute to this result is the presence of cationic vacancy in the Mn site.

The comparison of the results of the different crystal systems reveals that bond length decreases by approximately 0.020 Å (from 1.964 Å for LSM1 to 1.945 Å for LSM3) and that the bond angle increases by approximately 3° (from 164° for LSM1 to 167° for LSM3). The decrease in the Mn—O bond length with the increase in strontium content in the crystalline lattice indicates that part of the Mn^{3+} oxidizes to form Mn^{4+}. Probably, oxidation does not occur in the same extent as the increase in doping because the decrease in Mn—O is smaller than the variation in the average radius expected with doping for the B site. This indicates that the increasing in doping content not only oxidizes Mn, increasing the amount of cationic vacancy in the Mn site, but it probably also decreases the oxygen over stoichiometry found in $LaMnO_3$. These effects should contribute for stabilizing the charge defects and explain the XRD results [35,37].

Table 1 also presents the relative amounts of the phases present in the sample obtained by Rietveld refinement.

ICP-MS results obtained for LSM1, LSM2 and LSM3 samples are given in Table 2. The La, Sr and Mn percent values ($\%_{m/m}$) are associated to the total amount of those elements in the sample, and the elements ratio (mol) is given only for the elements in the perovskite structure. Even if the perovskite sample presents second phases, it is possible to determine its stoichiometry by Rietveld refinement process, as was observed with sample LSM3.

The reduction profile (TPR) of LSM samples is presented in Fig. 3. At least two reduction stages were found: the first at range 573–823 K and the second stage in the wide temperature interval of 923–1073 K. As Mn is the only reducible species in the case of lanthanum manganate doped strontium, this profile indicates the existence of two distinct manganese sites, Mn^{3+} and Mn^{4+}, in which the Mn^{4+} state reduces at a lower temperature as compared to Mn^{3+} [39,40]. It has been observed that reduction temperature decreases with strontium concentration increase, denoting the A site influence on Mn—O energy bond. The higher the strontium doping, the easier it is to break the Mn—O bond. Table 3 shows the area values and the corresponding reduction temperatures which were taken at the maximum of the each peak.

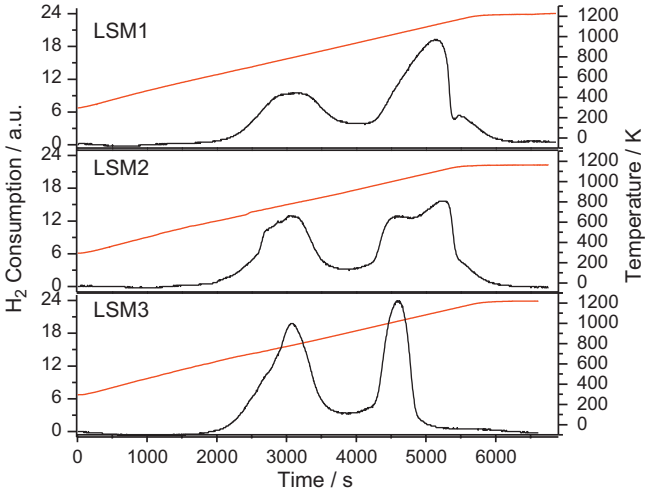

Fig. 3. TPR profile of samples synthesized by citrate route.

Table 3
Results of TPR analysis for LSM samples.

	Reduction (K)		Total areas (au)
LSM1	793[a]	1119[b]	29,739
LSM2	781[a]	1108[b]	30,273
LSM3	779[a]	1019[b]	27,321
CuO (standard)	621		42,696

[a] Peaks at lower temperatures (<873 K).
[b] Peaks at higher temperatures (>873 K).

After the reduction process, all initial manganese species (Mn^{3+} and Mn^{4+}) change into a bivalent state. In this case, it is not possible to determine the Mn^{3+} and Mn^{4+} ratio using the peaks area ratio as was done in other papers with different oxide [45] because some amount of Mn^{3+} can be reduced in the first reduction peak [39]. Then, it is necessary to take into account the standard sample (CuO) and the total area of the reduction peaks.

In this case it is indispensable to associate TPR and ICP results to quantify Mn^{3+} and Mn^{4+} using the following system:

$$\begin{cases} x + 2y \text{ is the total area of TPR profile} \\ x + y \text{ is the total manganese amount given from ICP results} \end{cases}$$

where *x* is Mn^{3+} amount and *y* is Mn^{4+} amount.

A similar system was used to estimate Mn^{4+} percentage from redox titration method. The results are given in Table 4.

The Mn^{4+} percentages obtained from these two different methods are quite close, which suggests that both methods are viable to quantify the Mn^{3+} and Mn^{4+} species.

Considering the ICP, TPR and redox titration results the perovskite chemical formulas have been estimated. The main assumptions concerned: (i) the oxygen amount needed for the charge electro neutrality and, (ii) the proportion of the elementary species, considered without excess at all sites. Many authors simplify the perovskite chemical formula by writing $LaSrMnO_{3+\delta}$, with an excess in the oxygen site but it must be emphasized that the real situation is the occurrence of vacancies at the cationic sites.

Table 4
Manganese percentage estimated by redox titration and TPR.

		LSM1	LSM2	LSM3
% Mn^{4+}	Titration	55	59	33
	TPR	58	65	34

The probable perovskite chemical formulas obtained after normalization can be represented as follows:

From TRP results:

LSM1: $(La_{0.82}Sr_{0.15}\square_{0.03})[Mn^{3+}_{0.39}Mn^{4+}_{0.52}\square_{0.09}]O_{3.00}$ MM = 227 g mol^{-1}

LSM2: $(La_{0.76}Sr_{0.18}\square_{0.06})[Mn^{3+}_{0.32}Mn^{4+}_{0.60}\square_{0.08}]O_{3.00}$ MM = 223 g mol^{-1}

LSM3: $(La_{0.58}Sr_{0.39}\square_{0.03})[Mn^{3+}_{0.66}Mn^{4+}_{0.34}]O_{2.93}\square_{0.07}$ MM = 220 g mol^{-1}

or/and

Considering redox tritation results:

LSM1: $(La_{0.82}Sr_{0.15}\square_{0.03})[Mn^{3+}_{0.41}Mn^{4+}_{0.50}\square_{0.09}]O_{3.00}$ MM = 228 g mol^{-1}

LSM2: $(La_{0.77}Sr_{0.19}\square_{0.05})[Mn^{3+}_{0.38}Mn^{4+}_{0.55}\square_{0.07}]O_{3.00}$ MM = 224 g mol^{-1}

LSM3: $(La_{0.58}Sr_{0.39}\square_{0.03})[Mn^{3+}_{0.67}Mn^{4+}_{0.33}]O_{2.93}\square_{0.07}$ MM = 219 g mol^{-1}

In these formulas the symbol □ denotes vacancy sites, and, MM is the compound molar mass. The occurrence of vacancies at other sites besides those mentioned here is possible, but it has not been considered.

The Mn^{4+} amounts found for LSM1 and LSM2 are much greater than those expected from the doping reaction, probably due to the high concentration of cationic vacancies. Contrarily, the LSM3 sample has less Mn^{4+} amounts than expected, less cationic vacancies and it is substoichiometric in oxygen. It seems that the trigonal phase has a Sr–host behavior better than the orthorhombic one.

It is known that when lanthanum manganite is doped strontium, the electroneutrality of the LSM is preserved with manganese oxidation or oxygen vacancies creation. Both processes can occur simultaneously, but one of them can predominate depending on the synthesis route, calcinations process and other preparation conditions [46,47]. The overall reactions are written in the Kröger–Vink notation:

(a) $2SrO + \frac{1}{2}O_{2(g)} \xrightarrow{LaMnO_3} 2Sr'_A + Mn^{\bullet}_B + 3O^{\times}_O$

(b) $2SrO \xrightarrow{LaMnO_3} 2Sr'_A + Mn^{\times}_B + 5O^{\times}_O + V^{\bullet\bullet}_O$

It is noted that the Sr concentration increasing for samples LSM1 and LSM2 increased Mn^{4+} from 0.52 to 0.60 and from 0.50 to 0.55 for TPR and titration results, respectively. The first process predominated in LSM1 and LSM2 and the second had a greater influence on LSM3.

4. Conclusions

The lanthanum manganites prepared by amorphous citrate route present a granular morphology after calcination at 1473 K which seems to be the ideal calcination temperature for samples prepared by citrate route. Monophase perovskite was found for LSM1 and LSM2 samples but one additional $La(OH)_3$ phase was observed for LSM3. Rietveld analysis showed that the weight percentage of this hydroxide phase is about 6%. Both oxides and hydroxides phases are described to be found in previous works mainly when crystallographic data are more accurately treated. Rietveld refinement provides the concentration of the secondary phases, therefore enables to determine the perovskite stoichiometry. The crystallographic structure of lanthanum manganites is dependent on the strontium content and although the system $La_{1-x}Sr_xMnO_3$ has a larger x range of formation of solid solution, the crystallographic structures are not the same for all x ranges.

XRD results also show that the insertion of strontium on lanthanium manganite structure causes the oxidation of Mn^{3+} into Mn^{4+} producing lattice modifications mainly for the parameter a which is related to the distance of the Mn—O bonds that decrease with the Sr content. As the Mn^{4+} ions (0.530 Å) are smaller than Mn^{3+} ions (0.645 Å), this parameter can also be used to indicate to what extend Mn^{3+} oxidation occurs during Sr doping.

The ratio Mn^{3+}/Mn^{4+} estimated by both temperature programmed reduction and redox titration decreases with the Sr-concentration for LSM1 and LSM2 samples. A Mn^{3+}/Mn^{4+} ratio closer to 1 was obtained for LSM1 which indicates the higher application potential of these sample compositions for using as SOFC–cathode materials since this ratio gives, at least theoretically, the best electronic conductivity.

Acknowledgments

This work was supported by CNPq, CAPES, FAPEMIG, FINEP and CEMIG.

References

[1] M.C. Brant, L. Dessemond, Solid State Ionics 138 (2000) 1–17.
[2] D. Stöver, H.P. Buchkremer, S. Uhlenbruck, Ceram. Int. 30 (2004) 1107–1113.
[3] D.Z.D. Florio, F.C. Fonseca, E.N.S. Muccillo, R. Muccillo, Cerâmica 50 (2004) 275–290.
[4] S.J. Stephen, Int. J. Inorg. Mater. 3 (2001) 113–121.
[5] T. Horita, K. Yamaji, N. Sakai, Y. Xiong, T. Kato, H. Yokokawa, T. Kawada, J. Power Sources 106 (2002) 224–230.
[6] E.P. Murray, T. Tsai, S.A. Barnett, Solid State Ionics 110 (1998) 235–243.
[7] A. Barbucci, R. Bozzo, G. Cerisola, P. Costamagna, Electrochim. Acta 47 (2002) 2183–2188.
[8] A. Barbucci, P. Carpanese, G. Cerisola, M. Viviani, Solid State Ionics 176 (2005) 1753–1758.
[9] A. Barbucci, M. Viviani, P. Carpanese, D. Vladikova, Z. Stoynov, Electrochim. Acta 51 (2006) 1641–1650.
[10] J. Deseure, Y. Bultel, L. Dessemond, E. Siebert, Electrochim. Acta 50 (2005) 2037–2046.
[11] V.V. Srdić, R.P. Omorjan, J. Seydel, Mater. Sci. Eng. B 116 (2005) 119–124.
[12] X. Deng, A. Petric, J. Power Sources 140 (2005) 297–303.
[13] H.Y. Jung, W.S. Kim, S.H. Choi, H.C. Kim, J. Kim, H.W. Lee, J.H. Lee, J. Power Sources 155 (2006) 145–151.
[14] X.J. Chen, K.A. Khor, S.H. Chan, J. Power Sources 123 (2003) 17–25.
[15] M. Kuznecov, P. Otschik, P. Obenaus, K. Eichler, W. Schaffrath, Solid State Ionics 157 (2003) 371–378.
[16] Y. N. Lee, Perovskitas sustituidas Ln1-xAxMnO3+d (Ln = La, Nd; A = K, Sr): síntesis por vías no convencionales, propiedades catalíticas y de magnetotransporte, PhD thesis, Universidad de València, València, 1997.
[17] F.W. Poulsen, Solid State Ionics 129 (2000) 145–162.
[18] P. Ciambelli, S. Cimino, L. Lisi, M. Faticanti, G. Minelli, I. Pettiti, P. Porta, Appl. Catal. B 33 (2001) 193–203.
[19] J.H. Kuo, H.U. Anderson, D.M. Sparlin, J. Solid State Chem. 87 (1990) 55–63.
[20] E. Siebert, A. Hammouche, M. Kleitz, Electrochim. Acta 40 (1995) 1741–1753.
[21] A. Hammouche, Contribution a l'etude de $La_{1-x}Sr_xMnO_3$ comme materiau d'electrode a oxygene a haute temperature, PhD thesis, L'Institut National Polytechnique de Grenoble, Grenoble, 1989, pp. 122.
[22] N. Caillol, M. Pijolat, E. Siebert, Appl. Surf. Sci. 253 (2007) 4641–4648.
[23] R. von Helmolt, J. Wecker, B. Holzapfel, L. Schultz, K. Samwer, Phys. Rev. Lett. 71 (1993) 2331–2333.
[24] A.P. Ramirez, J. Phys.: Condens. Matter 9 (1997) 8171–8199.
[25] J.M.D. Coey, M. Viret, S. von Molnar, Adv. Phys. 48 (1999) 167–293.
[26] M.B. Salamon, M. Jaime, Rev. Mod. Phys. 73 (2001) 583–628.
[27] K.-I. Chahara, T. Ohno, M. Kasai, Y. Kozono, Appl. Phys. Lett. 63 (1993) 1990–1992.
[28] S. Jin, T.H. Tiefel, R.A. McCormack, R. Ramesh, L.H. Chen, Science 264 (1994) 413–415.
[29] P. Mandal, S. Das, Phys. Rev. B 6 (1997) 15073–15080.
[30] P. Raychaudhuri, S. Mukherjee, A.K. Nigam, J. John, U.D. Vaisnav, R. Pinto, P. Mandal, J. Appl. Phys. 86 (1999) 5718–5725.
[31] J.S. Kang, Y.J. Kim, B.W. Lee, C.G. Olson, B.I. Min, J. Phys.: Condens. Matter 13 (2001) 3779–3784.
[32] G.T. Tan, S.Y. Dai, P. Duan, Y.L. Zhou, H.B. Lu, Z.H. Chen, J. Appl. Phys. 93 (2003) 5480–5483.
[33] L.C.M. Pinto, Quantikov, Belo Horizonte, CDTN 2005.
[34] J. Yang, W.H. Song, Y.Q. Ma, R.L. Zhang, Y.P. Sun, J. Magn. Magn. Mater. 285 (2005) 417–421.
[35] R. Bindu, Eur. Phys. J. B 37 (2004) 321–327.
[36] B.C. Tofield, W.R. Scott, J. Solid State Chem. 10 (1974) 183–194.
[37] M. Gaudon, C. Laberty-Robert, F. Ansart, Solid State Sci. 4 (2002) 125–133.

[38] H.Y. Hwang, S.W. Cheong, P.G. Radaelli, M. Marezio, B. Batlogg, Phys. Rev. Lett. 75 (1995) 914–917.
[39] F.C. Buciuman, F. Patcas, J. Zsakó, J. Therm. Anal. Calorim. 61 (2000) 819–825.
[40] F. Patcas, F.C. Buciuman, J. Zsako, Thermochim. Acta 360 (2000) 71–76.
[41] A. Ghosh, A.K. Sahu, A.K. Gulnar, A.K. Suri, Scr. Mater. 52 (2005) 1305–1309.
[42] R.J. Bell, G.J. Millar, J. Drennan, Solid State Ionics 131 (2000) 211–220.
[43] R. Marques, H. Zorel, M. Crespi, M. Jafelicci, C. Paiva-Santos, L. Varanda, R. Godoi, J. Therm. Anal. Calorim. 56 (1999) 143–149.
[44] P. Fleming, R.A. Farrell, J.D. Holmes, M.A. Morris, J. Am. Ceram. Soc. 93 (2010) 1187–1194.
[45] O. M'Ramadj, B. Zhang, D. Li, X. Wang, G. Lu, J. Nat. Gas Chem. 16 (2007) 258–265.
[46] A. Barnabé, M. Gaudon, C. Bernard, C. Laberty, B. Durand, Mater. Res. Bull. 39 (2004) 725–735.
[47] A.N. Grundy, E. Povoden, T. Ivas, L.J. Gauckler, J. Phase Equilib. 30 (2006) 33–41.